

# A Reinforcement Discrete Neuro-Adaptive Control for Unknown Piezoelectric Actuator Systems With Dominant Hysteresis

Chih-Lyang Hwang and Chau Jan

**Abstract**—The theoretical and experimental studies of a reinforcement discrete neuro-adaptive control for unknown piezoelectric actuator systems with dominant hysteresis are presented. Two separate nonlinear gains, together with an unknown linear dynamical system, construct the nonlinear model (NM) of the piezoelectric actuator systems. A nonlinear inverse control (NIC) according to the learned NM is then designed to compensate the hysteretic phenomenon and to track the reference input without the risk of discontinuous response. Because the uncertainties are dynamic, a recurrent neural network (RNN) with residue compensation is employed to model them in a compact subset. Then, a discrete neuro-adaptive sliding-mode control (DNASMC) is designed to enhance the system performance. The stability of the overall system is verified by Lyapunov stability theory. Comparative experiments for various control schemes are also given to confirm the validity of the proposed control.

**Index Terms**—Hysteresis, learning law with projection, piezoelectric actuator, recurrent neural network (RNN), sliding-mode control.

## I. INTRODUCTION

**H**YSTERESIS is nondifferential, multivalued, usually unknown, and commonly existing in physical systems [1]–[10], e.g., piezoelectric actuator. There are many applications using piezoelectric actuators, e.g., rotor bearing [1], diamond turning [8], scanning accuracy [2], vibration suppression [4], grinding table [5], microlithography [9]. The existence of hysteresis often severely limits the performance of the piezoelectric actuator, e.g., undesirable oscillation or even instability. Hence, how to design an effective controller for dealing with the hysteretic feature becomes a very important topic.

Cruz-Hernandez and Hayward [7] introduce a variable phase, an operator that shifts its periodic input signal by a phase angle that depends on the magnitude of the input signal. However, this study must redesign for different piezoelectric actuators. Tao and Kokotovic [3] use a simplified hysteresis model that captures most of the hysteresis characteristic; the design uses an adaptive hysteresis inverse cascade with the system so that the system becomes a linear structure with uncertainties. However, the linear dynamic system must satisfy some assumptions, e.g.,

Manuscript received January 4, 2001; revised September 5, 2001 and April 22, 2002. This work was supported by the National Science Council, R.O.C., under Grant NSC-89-2212-E-036-008.

The authors are with the Department of Mechanical Engineering, Tatung University, Taipei 10451, Taiwan, R.O.C. (e-mail: clhwang@ttu.edu.tw).

Digital Object Identifier 10.1109/TNN.2002.806610

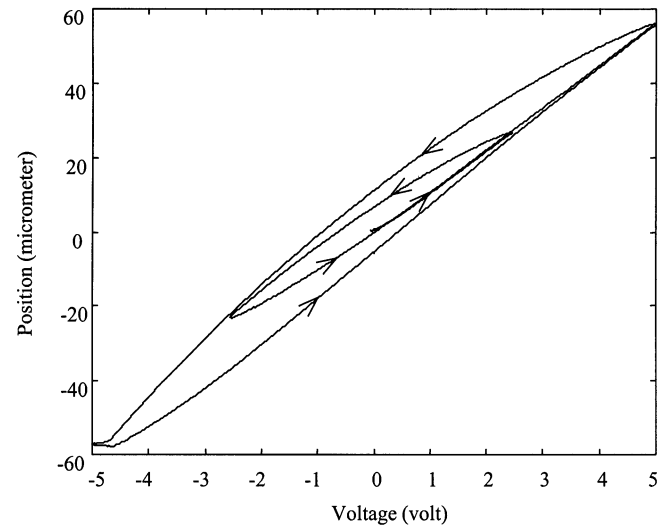


Fig. 1. Hysteresis characteristic.

minimum phase system, known relative degree. Ge and Jouaneh [6] discuss a comparison between a forward control, a regular proportional integral derivative (PID) control and a PID feedback control with hysteretic modeling in the feedforward loop. The result shows that the tracking control performance is greatly improved by augmenting the feedback loop with a model of hysteresis in the feedforward loop. However, the result is only valid for tracking a sinusoidal trajectory.

Because the different polarity or amplitude of the input signal causes the different hysteretic loop (cf. Fig. 1 for various operating ranges of piezoelectric actuator), an effective nonlinear inverse control (NIC) is difficult to design. Under the circumstances, a NIC is constructed to prevent a discontinuous response and to partially cancel the nonlinearity of hysteresis (e.g., [10], [11]). Only the remaining uncertainty is required to learn by a neural network. The system performance is better than that using the learning of whole nonlinear dynamics (e.g., [12]). This is one of the motivations of this study.

Because the remaining uncertainty is dynamic, a suitable recurrent neural network (RNN) is easily designed to improve the approximation online. A RNN can cope with time-varying input or output through its own natural temporal operation. Hence, the same number of neurons used for the RNN, can model the dynamic uncertainties to achieve the required accuracy [12]–[15]. Then, an online RNN with residue compensation is designed to deal with the remaining dynamic uncertainties. This is the second motivation of the study.

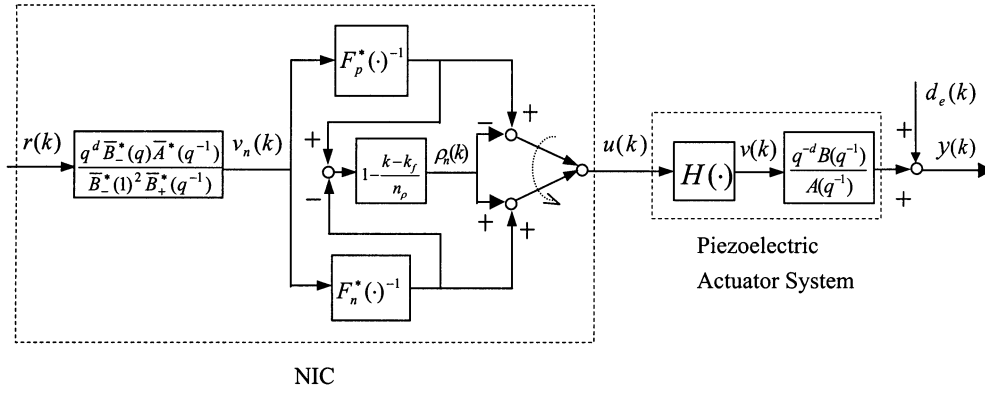


Fig. 2. Block diagram of nonlinear inverse control.

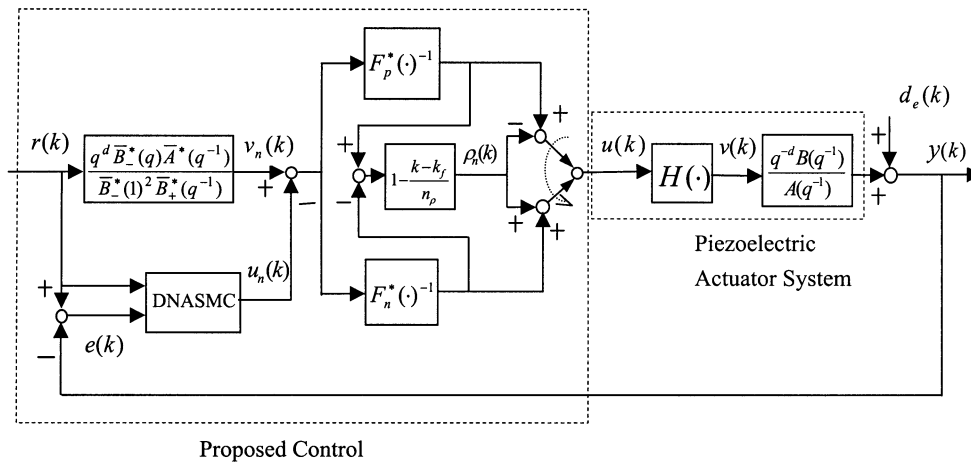


Fig. 3. Block diagram of the proposed control.

Without the requirement of persistent excitation, a learning law with projection is given to guarantee the boundedness of the learning weight with adjustable convergent rate. The initial values of weight can be set to zero (i.e., no compensation for the uncertainty with respect to robust control). This characteristic makes the suggested control more practical, because many neural-network controls are difficult to assign an initial value for the connection weight (e.g., [13] and [14]). Then a discrete neuro-adaptive sliding-mode control (DNASMC) is constructed to improve the system performance. This is the third motivation of the paper. Finally, the comparative experiments (for the open-loop control, PID control, NIC, NIC + PID control, and the proposed control system) are arranged to verify the effectiveness of the proposed control.

## II. NIC AND TRACKING ERROR MODEL

In Section II-A, a nonlinear model (NM) for hysteresis is introduced. In Section II-B, a NIC is given. In Section II-C, a tracking error model resulting from the proposed NIC is derived.

### A. NM for Hysteresis

Consider the following unknown systems with dominant hysteresis:

$$v(k) = H[u(k)] \quad (1a)$$

$$y(k) = q^{-d} \frac{B(q^{-1})v(k)}{A(q^{-1})} \quad (1b)$$

where  $y(k)$  and  $u(k)$  denote the system output and input,  $H(\cdot)$  represents an unknown hysteresis (cf. Fig. 1),  $v(k)$  stands for the output of hysteresis which is unavailable,  $d \geq 1$  is a known time delay,  $q^{-1}$  denotes the backward-time shift operator, and  $A(q^{-1})$  and  $B(q^{-1})$  denote two unknown coprime polynomials but  $A(q^{-1})$  is stable and monic.

A NM is first employed to learn the hysteretic behavior of the piezoelectric actuators. Without the risk of abrupt response, a NIC (cf. Fig. 2) based on the learned NM is designed to approximately cancel the unknown hysteresis and to attain an acceptable tracking performance. After an approximate cancellation of hysteresis and a design of trajectory tracking, a DNASMC is constructed to tackle the resulting linear tracking error dynamic system with uncertainties (cf. Fig. 3). The main feature of DNASMC is to use an on-line RNN with residue compensation to approximate a possibility of enormous uncertainty caused by the modeling error (e.g., different polarity or amplitude of the input, or an external load) and learning law. Without the condition of persistent excitation for the basis function of RNN, a learning law with projection is also designed to ensure the boundedness of the learning weight with adjustable convergent rate.

### B. NIC

There often has an NIC for a controlled system with hard nonlinearity (cf. [10], [11]). Here, the following NM (e.g., [10]) is first considered:

$$v_n(k) = \frac{1 + \bar{c}_1(k)\bar{c}_3(k) - z(k)}{\bar{c}_1(k)[1 + z(k)]} = F(u, \bar{c}_1, \bar{c}_2, \bar{c}_3) \quad (2)$$

$$y_n(k) = - \sum_{i=1}^{\bar{n}_a} \bar{a}_i(k-1)y_n(k-i) + \sum_{i=1}^{\bar{n}_b} \bar{b}_i(k-1)v_n(k-i-d+1) \quad (3)$$

where

$$z(k) = e^{-2\bar{c}_1(k)[u(k)-\bar{c}_2(k)]}. \quad (4)$$

The weights  $\bar{a}_i(k)$ ,  $\bar{b}_j(k)$  for  $i = 1, 2, \dots, \bar{n}_a$ ,  $j = 0, 1, \dots, \bar{n}_b$  and  $\bar{c}_j(k)$  for  $j = 1, 2, 3$  are achieved by an offline learning. In addition, the signals  $v_n(k)$  and  $y_n(k)$  denote the output of an estimated nonlinear static and dynamic model of hysteresis in (1a) and (1b), respectively. It should be noted that the hysteresis is approximated by two nonlinear functions in (2), according to the change rate (or polarity) and the amplitude of the  $u(k-1)$ . That is, an optimal model to approximate the dynamics of (1) is described as follows:

$$\bar{a}_i(k) = \bar{a}_i^*, \quad \bar{b}_j(k) = \bar{b}_j^*, \quad i = 1, 2, \dots, \bar{n}_a; \quad j = 0, 1, \dots, \bar{n}_b \quad (5)$$

$$\bar{c}_j(k) = \begin{cases} \bar{c}_{pj}^*, & \text{as } \Delta u(k-1) \geq 0 \\ \bar{c}_{nj}^*, & \text{as } \Delta u(k-1) < 0 \end{cases}, \quad j = 1, 2, 3 \quad (6)$$

where  $\Delta u(k-1) = u(k-1) - u(k-2)$ ,  $\bar{a}_i^*$ ,  $\bar{b}_j^*$  for  $i = 1, 2, \dots, \bar{n}_a$ ,  $j = 0, 1, \dots, \bar{n}_b$ ,  $\bar{c}_{pj}^*$ ,  $\bar{c}_{nj}^*$  for  $j = 1, 2, 3$  are not necessarily unique and dependent on the amplitude of the input signal. Generally,  $\bar{n}_a < n_a$ ,  $\bar{n}_b < n_b$ . The modeling of the nonlinear model can refer to [10].

After effective learning and model verification, a suitable order of the system (1) can be determined. Under this circumstance, the nonlinear function in (2) becomes a function of  $u(k)$

only. Its inverse function  $F^*(v_n)^{-1}$  for positive and negative  $\Delta u(k-1)$  are described as follows:

$$F_p^*(v_n)^{-1} = \bar{c}_{p2}^* - \frac{1}{2\bar{c}_{p1}^*} \log \left[ \frac{1 + \bar{c}_{p1}^* \bar{c}_{p3}^* - \bar{c}_{p1}^* v_n(k)}{1 + \bar{c}_{p1}^* v_n(k)} \right] \quad (7)$$

$$F_n^*(v_n)^{-1} = \bar{c}_{n2}^* - \frac{1}{2\bar{c}_{n1}^*} \log \left[ \frac{1 + \bar{c}_{n1}^* \bar{c}_{n3}^* - \bar{c}_{n1}^* v_n(k)}{1 + \bar{c}_{n1}^* v_n(k)} \right]. \quad (8)$$

For simplicity, an optimal set of  $\bar{c}_{pj}^*$ ,  $\bar{c}_{nj}^*$  for  $j = 1, 2, 3$  is chosen for the possible amplitude of the input signal. Based on the concept of inverse control and zero-phase tracking control, the following NIC (cf. Fig. 2) without the risk of discontinuous response is accomplished as shown in (9) and (10) at the bottom of the page, where  $k_f$  is defined as the time  $k$  that  $\text{sgn}[\Delta u(k-2)] \neq \text{sgn}[\Delta u(k-1)]$  and

$$v_n(k) = \frac{[q^d \bar{B}_-(q) \bar{A}^*(q^{-1})] r(k)}{[\bar{B}_-(1)^2 \bar{B}_+(q^{-1})]} \quad (11)$$

where  $\bar{A}^*(q^{-1})$  is stable and monic and the notations of  $\bar{B}_+(q^{-1})$ ,  $\bar{B}_-(q^{-1})$  denote the stable and unstable part of  $\bar{B}^*(q^{-1})$ , respectively. As the discontinuity of nonlinear model is large,  $n_p$  is chosen as a large integer. That is, an improvement  $\rho_n(k)$  in (10) reduces the hysteretic error caused by the discontinuity of the model.

### C. Tracking Error Model

The NIC not only approximately cancels the hysteretic effect but also tracks a trajectory with following result:

$$e(k) = \frac{[B(q^{-1})e_h(k-d)]}{A(q^{-1})} + e_{ze}(k) + d_e(k) \quad (12)$$

where  $r(k)$  is the reference input and  $e(k) = r(k) - y(k)$ ,  $d_e(k)$  denotes an external disturbance that is relatively bounded, and we have (13) and (14), shown at the bottom of the page. The signal  $e_{ze}(k)$  denotes the uncertainties caused by the forward control, and the symbol  $e_h(k-d)$  denotes the uncertainties caused by the approximation of hysteresis. Because an accurate modeling of unknown system with hysteresis is difficult to obtain, the tracking error based on NIC is generally not superior

$$u(k) = \begin{cases} F_p^*(v_n)^{-1} - \rho_n, & \text{as } \Delta u(k-1) \geq 0 \\ F_n^*(v_n)^{-1} = \rho_n, & \text{as } \Delta u(k-1) < 0 \end{cases} \quad (9)$$

$$\rho_n(k) = \begin{cases} [F_p^*(v_n)^{-1} - F_n^*(v_n)^{-1}] \left[ \frac{1-(k-k_f)}{n_p} \right], & k_f \leq k \leq k_f + n_p \\ 0, & \text{otherwise} \end{cases} \quad (10)$$

$$e_{ze}(k) = \frac{[A(q^{-1})\bar{B}_+(q^{-1})\bar{B}_-(1)^2 - \bar{A}^*(q^{-1})B(q^{-1})\bar{B}_-(q)] r(k)}{[A(q^{-1})\bar{B}_+(q^{-1})\bar{B}_-(1)^2]} \quad (13)$$

$$e_h(k-d) = F^*(u(k-d)) - H(u(k-d)). \quad (14)$$

[1]–[10]. To compensate these phenomena, a DNASMC is affiliated with the previous NIC (cf. Fig. 3). Then the error-model of closed-loop system in Fig. 3 is depicted as follows:

$$\begin{aligned} A(q^{-1})[e(k) - e_{ze}(k) - d_e(k)] \\ = B(q^{-1})[u_n(k-d) + e_h(k-d)]. \end{aligned} \quad (15)$$

The subsequent work is to design a DNASMC  $u_n(k-d)$  so that  $e(k)$  is as small as possible under the uncertainties  $e_{ze}(k)$  and  $e_h(k-d)$ , the unknown polynomials  $A(q^{-1})$ ,  $B(q^{-1})$ , and an external disturbance  $d_e(k)$ . Before designing the DNASMC, the following upper bound of the approximation error of hysteresis [cf. (14)] is estimated:

$$\begin{aligned} A1: |e_h(k)| \leq \delta_0 + \delta_1 |u(k)|, \\ \text{where } \delta_0 \text{ and } \delta_1 \geq 0 \text{ are known.} \end{aligned} \quad (16)$$

First, one rewrites (15) into a state-space form

$$\begin{aligned} X(k+1) = [\bar{A}^* + \Delta A] X(k) + [\bar{B}^* + \Delta B] \\ \times [u_n(k-d+1) + e_h(k-d+1)] \end{aligned} \quad (17)$$

$$e(k) = [\bar{C}^* + \Delta C] X(k) + e_{ze}(k) + d_e(k) \quad (18)$$

where the triplex  $(\bar{A}^*, \bar{B}^*, \bar{C}^*)$  corresponds to the nominal (or optimal) system of (15) which is known, observable, and controllable, the triplex  $[\Delta A, \Delta B, \Delta C]$  corresponds to the uncertainties caused by the difference between the linear nominal system and unknown linear system. For instance, the nominal system of (17) and (18) is written as the following observable canonical form:

$$\begin{aligned} \bar{A}^* = \begin{bmatrix} -\bar{a}_1^* & 1 & & \\ -\bar{a}_2^* & & \ddots & \\ \vdots & & & 1 \\ -\bar{a}_n^* & & & 0 \end{bmatrix}, \quad \bar{B}^* = \begin{bmatrix} \bar{b}_0^* \\ \bar{b}_1^* \\ \vdots \\ \bar{b}_{n-1}^* \end{bmatrix} \\ \bar{C}^* = \begin{bmatrix} 1 \\ 0 \\ \vdots \\ 0 \end{bmatrix}^T \end{aligned} \quad (19)$$

where  $n = \max[n_a, d + n_b - 1]$ . The system state can be represented by the combination of  $e(k), \dots, e(k-n+1), u_n(k-d), \dots, u_n(k-n-d)$  and the uncertainties  $[\Delta A, \Delta B, \Delta C]$ ,  $e_h(k-d)$ ,  $e_{ze}(k)$ , and  $d_e(k)$  [17]. That is

$$x_1(k) = (1 - \Delta C C^p) [e(k) - e_{ze}(k) - d_e(k)] \quad (20)$$

$$\begin{aligned} x_i(k+1) = -\bar{a}_i^* e(k) + \bar{b}_{i-1}^* u_n(k-d+1) + x_{i+1}(k) \\ + \Delta \rho_i(k) \end{aligned}$$

$$x_{n+1}(k) = 0, \quad 2 \leq i \leq n \quad (21)$$

where

$$\begin{aligned} \Delta \rho_i(k) = -\Delta a_i (1 - \Delta C C^p) [e(k) - e_{ze}(k) - d_e(k)] \\ + \bar{a}_i^* [\Delta C C^p e(k) + (1 - \Delta C C^p) \\ \times (e_{ze}(k) + d_e(k))] \\ + [\bar{b}_{i-1}^* + \Delta b_{i-1}] e_h(k-d+1) \\ + \Delta b_{i-1} u_n(k-d+1) \end{aligned} \quad (22)$$

$$\begin{aligned} C^p = (\bar{C}^* + \Delta C)^T \\ \times \left\{ (\bar{C}^* + \Delta C) (\bar{C}^* + \Delta C)^T \right\}^{-1}. \end{aligned} \quad (23)$$

Because  $(\bar{C}^* + \Delta C) \neq 0$ , the scalar  $(\bar{C}^* + \Delta C)(\bar{C}^* + \Delta C)^T \neq 0$ . The recursive processing of (21) in backward direction yields

$$\begin{aligned} x_j(k+1) \\ = -\sum_{i=0}^{n-j} \{ \bar{a}_{i+j}^* e(k-i) - \bar{b}_{i+j-1}^* u_n(k-i+d-1) \} \\ + \sum_{i=0}^{n-j} \Delta \rho_{i+j}(k-i), \quad 2 \leq j \leq n. \end{aligned} \quad (24)$$

Together with (18) and (24), the following equation is achieved.

$$X(k) = \bar{G}^* Z(k) + \Delta G(e, u_n, r) \quad (25)$$

where we have (26)–(29), shown at the bottom of the page. Because the uncertainties  $\Delta g_i (2 \leq j \leq n)$  are functions of  $u_n$ , we must cope with them; i.e.,

$$\begin{aligned} \Delta g_2(e, u_n, r) = \{ \Delta C C^p [A_1(q^{-1}) + \Delta A_1(q^{-1})] \\ - \Delta A_1(q^{-1}) \} e(k) \\ + (1 - \Delta C C^p) \Delta A_1(q^{-1}) \\ \times (e_{ze}(k) + d_e(k)) \\ + [B_1(q^{-1}) + \Delta B_1(q^{-1})] \\ \times e_h(k-d+1) \\ + \Delta B_1(q^{-1}) u_n(k-d+1) \end{aligned} \quad (30)$$

$$Z(k) = [e(k) \quad \dots \quad e(k-n+1) \quad u_n(k-d) \quad \dots \quad u_n(k-n-d)]^T \quad (26)$$

$$\bar{G}^* = \begin{bmatrix} 1 & 0 & & & & & & 0 \\ 0 & -\bar{a}_2^* & & & -\bar{a}_n^* & \bar{b}_1^* & & \bar{b}_{n-1}^* \\ \cdot & -\bar{a}_3^* \dots & & -\bar{a}_n^* & 0 & \bar{b}_2^* \dots & & 0 \\ \cdot & \cdot & & \cdot & \cdot & \cdot & & \cdot \\ \cdot & \cdot & & \cdot & \cdot & \cdot & & \cdot \\ \cdot & -\bar{a}_{n-1}^* & -\bar{a}_n^* & 0 \dots & 0 & \bar{b}_{n-2}^* & \bar{b}_{n-1}^* & 0 \dots \\ 0 & -\bar{a}_n^* & 0 & \dots & 0 & \bar{b}_{n-1}^* & 0 & \dots \\ & & & & & & & 0 \end{bmatrix} \quad (27)$$

$$\Delta g_1(e, u_n, r) = -\Delta C C^p e(k) - (1 - \Delta C C^p) (e_{ze}(k) + d_e(k)) \quad (28)$$

$$\Delta g_j(e, u_n, r) = \sum_{i=0}^{n-j} \Delta \rho_{i+j}(k-i-1), \quad 2 \leq j \leq n. \quad (29)$$

where

$$\begin{aligned}\Delta A_1(q^{-1}) &= \Delta a_2 + \dots + \Delta a_n q^{-n+1} \\ A_1(q^{-1}) &= \bar{a}_2^* + \dots + \bar{a}_n^* q^{-n+1}\end{aligned}\quad (31)$$

$$\begin{aligned}\Delta B_1(q^{-1}) &= \Delta b_1 + \dots + \Delta b_{n-1} q^{-n+1} \\ B_1(q^{-1}) &= \bar{b}_1^* + \dots + \bar{b}_{n-1}^* q^{-n+1}.\end{aligned}\quad (32)$$

Similarly,  $\Delta g_i$  for  $i \geq 3$ . Those are omitted because they are not used for the controller analysis. The purpose of this subsection is to express the state in terms of tracking error, input, and uncertainty.

### III. DNASMC

In this section, we discuss the design of DNASMC.

#### A. RNN With Residue Compensation

The unknown nonlinear function  $\Gamma(x)$  can be described as follows (cf. [12]):

$$\Gamma(x) = \bar{W}_1^T \sigma(\bar{W}_2^T \bar{x}(k) + \bar{W}_3^T q^{-1}(\sigma)) + \varepsilon_f(\bar{x}). \quad (33)$$

*Remark 1:* The constant matrices in (33) are not unique and satisfy the following inequalities:  $\|\bar{W}_1\|_F \leq W_{1m}$ ,  $\|\bar{W}_2\|_F \leq W_{2m}$ ,  $0 \leq \|\bar{W}_3\|_F \leq W_{3m} < 1$  where  $W_{1m}$ ,  $W_{2m}$ , and  $W_{3m}$  are known, and  $\|W\|_F^2 = \text{tr}(W^T W) = \text{tr}(W W^T)$  denotes the Frobenius norm.

Then the following matrix-form approximator of RNN is given:

$$\begin{aligned}\hat{\Gamma}(\bar{x}, \hat{W}_1, \hat{W}_2, \hat{W}_3) \\ = \hat{W}_1^T(k) \sigma(\hat{W}_2^T(k) \bar{x}(k) + \hat{W}_3^T(k) q^{-1}(\hat{\sigma}))\end{aligned}\quad (34)$$

where  $\hat{W}_1^T(k)$ ,  $\hat{W}_2^T(k)$ ,  $\hat{W}_3^T(k)$  denote the corresponding learning weights of  $\bar{W}_1^T$ ,  $\bar{W}_2^T$ ,  $\bar{W}_3^T$ , and  $\hat{\sigma}(\bar{x}) = \sigma(\hat{W}_2^T(k) \bar{x}(k) + \hat{W}_3^T(k) q^{-1}(\hat{\sigma}))$ . The function approximation error  $\tilde{\Gamma} = \Gamma - \hat{\Gamma}$  in a linearly parameterized form of  $\tilde{W}_i(k) = \bar{W}_i - \hat{W}_i(k)$ , for  $i = 1, 2, 3$  that can be expressed as

$$\begin{aligned}\tilde{\Gamma}(\bar{x}, \hat{W}_1, \hat{W}_2, \hat{W}_3) &= \tilde{W}_1^T(k) \left\{ \hat{\sigma}(\bar{x}) - \hat{\sigma}'(\bar{x}) \hat{W}_2^T(k) \bar{x}(k) \right. \\ &\quad \left. - 2\hat{\sigma}'(\bar{x}) \hat{W}_3^T(k) q^{-1}(\hat{\sigma}) \right\} \\ &\quad + \hat{W}_1^T(k) \hat{\sigma}'(\bar{x}) \\ &\quad \times \left\{ \tilde{W}_2^T(k) \bar{x}(k) + 2\tilde{W}_3^T(k) q^{-1}(\hat{\sigma}) \right\} \\ &\quad + \tilde{\varepsilon}_f(k, \bar{x})\end{aligned}\quad (35)$$

where

$$\begin{aligned}\tilde{\varepsilon}_f(k, \bar{x}) &= \tilde{W}_1^T(k) \hat{\sigma}'(\bar{x}) \\ &\quad \times \left\{ \bar{W}_2^T \bar{x}(k) + \bar{W}_3^T(k) q^{-1}(\hat{\sigma}) \right. \\ &\quad \left. + \bar{W}_3^T q^{-1}(\hat{\sigma}) + \hat{W}_3^T(k) q^{-1}(\sigma) \right\} \\ &\quad + \hat{W}_1^T(k) \hat{\sigma}'(\bar{x}) \tilde{W}_3^T(k) q^{-1}(\sigma) + \bar{W}_1^T \\ &\quad \times O \left[ \tilde{W}_2^T(k) \bar{x}(k) + \tilde{W}_3^T(k) q^{-1}(\sigma) \right. \\ &\quad \left. + \hat{W}_3^T(k) q^{-1}(\hat{\sigma}) \right]^2 + \varepsilon_f(\bar{x})\end{aligned}\quad (36)$$

$$\begin{aligned}\sigma'(\bar{x}) &= \text{diag} \{ \sigma'_1(\bar{x}), \dots, \sigma'_\alpha(\bar{x}) \} \in \mathfrak{R}^{\alpha \times \alpha} \\ \sigma'_i(\bar{x}) &= \left. \frac{d\sigma(z)}{dz} \right|_{z=\bar{x}} = \sigma_i(\bar{x}) (1 - \sigma_i(\bar{x})), \\ &\quad 1 \leq i \leq \alpha.\end{aligned}\quad (37)$$

The approximation  $\hat{\Gamma}(\bar{x}, \hat{W}_1, \hat{W}_2, \hat{W}_3)$  is used in the control law to cancel the unknown nonlinear function  $\Gamma(x)$ . The first and second terms of  $\tilde{\Gamma}(\bar{x}, \hat{W}_1, \hat{W}_2, \hat{W}_3)$  is canceled (or improved) by the learning law of weights  $\hat{W}_1(k)$ ,  $\hat{W}_2(k)$  and  $\hat{W}_3(k)$ . Although the residue  $\tilde{\varepsilon}_f(k, \bar{x})$  is unknown, an upper bound of  $\|\tilde{\varepsilon}_f(k, \bar{x})\|$  can be achieved as follows (see [12]):

$$\|\tilde{\varepsilon}_f(k, \bar{x})\| \leq \bar{W}_4^T \Psi(k) \quad (38a)$$

where we have (38b), shown at the bottom of the page.

#### B. DNASMC

Define the following sliding surface with proportional and integral properties:

$$s(k) = \rho s(k-1) + \sum_{i=0}^{n_s} d_i e(k-i), \quad d_0 = 1 \quad (39)$$

where  $1^- \leq \rho \leq 1$ , the zero at  $1^-$  is employed to eliminate any constant in  $s(k)$  and the coefficients  $d_i$  ( $1 \leq i \leq n_s$ ) is chosen such that  $s(k) = 0$  is Hurwitz. In general,  $n_s \leq \bar{n}_\alpha$ .

Consider the following projection learning laws with adjustable convergent rate:

$$\hat{W}_i(k+1) = \hat{W}_i(k) + \Lambda_i(k) - P_i(k) \hat{W}_i(k), \quad i = 1, 2, 3, 4 \quad (40)$$

where we have (41)–(46), shown at the bottom of the next page, where  $\alpha_i > 0$ ,  $\beta_i(2 - \beta_i) - \mu_i > 0$ ,  $1 > \beta_i > \mu_i > 0$  for  $i = 1, 2, \dots, 4$ ,  $\gamma > 0$  and  $b$  is a known constant. The learning laws of weight matrices (40) have learning rates  $\alpha_i$  for  $i = 1, 2, \dots, 4$ , error function  $s(k)$ , and specific basis functions in  $\Lambda_i(k)$  for  $i = 1, 2, \dots, 4$  except  $\alpha_i$  and  $s(k)$ . In general, the learning rate (i.e.,  $\alpha_i$  for  $i = 1, 2, \dots, 4$ ) must be

$$\Psi(k) = \left[ 1 \quad \|\bar{x}(k)\| \quad \left\| \hat{W}_1(k) \right\|_F \quad \left\| \hat{W}_3(k) \right\|_F \quad \|\bar{x}(k)\| \left\| \hat{W}_1(k) \right\|_F \quad \|\bar{x}(k)\| \left\| \hat{W}_2(k) \right\|_F \quad \left\| \hat{W}_1(k) \right\|_F \left\| \hat{W}_3(k) \right\|_F \right]^T. \quad (38b)$$

chosen small enough to avoid the instability of the closed-loop system, as the number of weight is large [12]–[15]. The projection term  $P_i(k)\hat{W}_i(k)$  in (40) is used to guarantee that  $\|\hat{W}_i(k)\|_F < W_{im}$  as  $k \rightarrow \infty$  and a better convergent rate (via  $\beta_i$  for  $i = 1, 2, \dots, 4$ ) as compared with traditional learning law (e.g., [13]–[15]).

The following assumption is required for the derivation of the proposed DNASMC in Theorem 1, as shown in the last equation at the bottom of the page, where  $\beta$  is known,  $\Delta\beta = \bar{C}^*\Delta B + \Delta C[\bar{B}^* + \Delta B]$ , and  $|\bar{C}^*\bar{B}^*| \gg s_0 > 0$ .

The uncertainty  $\Gamma_u(k)$  caused by  $\Delta A$ ,  $\Delta B$ ,  $\Delta C$ ,  $e_h(k)$ ,  $e_{ze}(k)$ , and  $d_e(k)$  is expressed as follows:

$$\begin{aligned} \Gamma_u(k) = & \{[\Delta C\bar{A}^* + \bar{C}^*\Delta A + \Delta C\Delta A]C^p \\ & + \Delta C C^p [\bar{a}_1^* + A_1(q^{-1}) + \Delta A_1(q^{-1})] \\ & - \Delta A_1(q^{-1})\} e(k) \\ & + \{\Delta\beta + \Delta B_1(q^{-1}) + [(\bar{C}^* + \Delta C)(\bar{B}^* + \Delta B) \\ & + B_1(q^{-1}) + \Delta B_1(q^{-1})] \delta_1\} \\ & \times u_{eq}(k-d+1) \\ & + [(\bar{C}^* + \Delta C)(\bar{B}^* + \Delta B) + B_1(q^{-1}) \\ & + \Delta B_1(q^{-1})] \delta_0 \\ & + \{q - (\Delta C\bar{A}^* + \bar{C}^*\Delta A + \Delta C\Delta A)C^p \\ & + (1 - \Delta C C^p)[\bar{a}_1^* + \Delta A_1(q^{-1})]\} \\ & \times [e_{ze}(k) + d_e(k)] \end{aligned} \quad (47)$$

where  $C^p$  is described in (23). It is approximated by the following RNN:

$$\Gamma_u(k) = \bar{W}_1^T \sigma(\bar{W}_2^T \bar{\varphi}(k) + \bar{W}_3^T q^{-1}(\sigma)) + \varepsilon_u(\bar{\varphi}), \text{ as } \bar{\varphi}(k) \in \Omega \quad (48)$$

where  $|\varepsilon_u(\bar{\varphi})| < \varepsilon$ , as  $\bar{\varphi}(k) \in \Omega = \{\bar{\varphi} \mid \|\bar{\varphi} - \bar{\varphi}_0\|_{p,w} \leq 1\}$ , where  $\|\bar{\varphi}\|_{p,w} = \{\sum_{i=1}^n (\bar{\varphi}_i/w_i)^p\}^{1/p}$  and  $\bar{\varphi}_0$  denotes the absolute location of the set. The following uncertain signal  $R_{sw}(k)$  (without showing their arguments) derived from the difference of sliding surface, i.e.,  $\Delta s(k) = s(k+1) - s(k)$  (cf. (A4)), is required for the design of switching control (53) of DNASMC

$$\begin{aligned} R_{sw} = & \tilde{W}_1^T [\hat{\sigma} - \hat{\sigma}' \hat{W}_2^T \bar{\varphi} - 2\hat{\sigma}' \hat{W}_3^T q^{-1}(\hat{\sigma})] \\ & + \hat{W}_1^T \hat{\sigma}' [\tilde{W}_2^T \bar{\varphi} + 2\tilde{W}_3^T q^{-1}(\hat{\sigma})] + \tilde{\varepsilon}_f \\ & - \left[\frac{\Lambda_1^T}{2} - \beta_1 \hat{W}_1^T\right] [\hat{\sigma} - \hat{\sigma}' \hat{W}_2^T \bar{\varphi} - 2\hat{\sigma}' \hat{W}_3^T q^{-1}(\hat{\sigma})] \\ & - \hat{W}_1^T \hat{\sigma}' \left[\frac{\Lambda_2^T}{2} - \beta_2 \hat{W}_2^T\right] \bar{\varphi} \\ & - \hat{W}_1^T \hat{\sigma}' [\Lambda_3^T - 2\beta_3 \hat{W}_3^T] q^{-1}(\hat{\sigma}) \\ & - \frac{\alpha_4 s \Psi^T \Psi}{4} - \frac{(1 - \beta_4) s \hat{W}_4^T \Psi}{|s|}. \end{aligned} \quad (49)$$

Taking the norm of (49) by using the result of Remark 1 gives the following upper bound the uncertain signal  $G_{sw}(k)$ :

$$\begin{aligned} |R_{sw}| \leq G_{sw} = & [W_{1m} + (1 - \eta_1) \|\hat{W}_1\|_F] \\ & \times \|\hat{\sigma} - \hat{\sigma}' \hat{W}_2^T \bar{\varphi} - 2\hat{\sigma}' \hat{W}_3^T q^{-1}(\hat{\sigma})\| \\ & + [W_{2m} + (1 - \beta_2) \|\hat{W}_2\|_F] \|\hat{W}_1^T \hat{\sigma}'\| \|\bar{\varphi}\| \\ & + 2 [W_{3m} + (1 - \beta_3) \|\hat{W}_3\|_F] \|\hat{W}_1^T \hat{\sigma}'\| \\ & \times \|q^{-1}(\hat{\sigma})\| \\ & + [W_{4m} + (1 - \beta_4) \|\hat{W}_4\|_F] \|\Psi\| + |s| \end{aligned}$$

$$\Lambda_1(k) = \frac{\alpha_1 s(k) [\hat{\sigma}(\bar{\varphi}) - \hat{\sigma}'(\bar{\varphi}) \hat{W}_2^T(k) \bar{\varphi}(k) - 2\hat{\sigma}'(\bar{\varphi}) \hat{W}_3^T(k) q^{-1}(\hat{\sigma})]}{2} \quad (41)$$

$$\Lambda_2(k) = \frac{\alpha_2 s(k) \bar{\varphi}(k) \hat{W}_1^T(k) \hat{\sigma}'(\bar{\varphi})}{2} \quad (42)$$

$$\Lambda_3(k) = \alpha_3 s(k) \hat{\sigma}'(\bar{\varphi}) q^{-1}(\hat{\sigma}) \hat{W}_1^T(k) \quad (43)$$

$$\Lambda_4(k) = \frac{\alpha_4 |s(k)| \Psi(k)}{2} \quad (44)$$

$$P_i(k) = \begin{cases} \beta_i \hat{W}_i(k), & \text{if } \|\hat{W}_i(k)\|_F < W_{im}, \text{ or if } \|\hat{W}_i(k)\|_F \geq W_{im}, \text{tr} [\Lambda_i^T(k) \hat{W}_i(k)] \leq 0 \\ \frac{\beta_i \hat{W}_i(k) + \text{tr}[\Lambda_i^T(k) \hat{W}_i(k)]}{[\gamma + \|\hat{W}_i(k)\|_F^2]}, & \text{if } \|\hat{W}_i(k)\|_F \geq W_{im}, \text{tr} [\Lambda_i^T(k) \hat{W}_i(k)] > 0 \end{cases} \quad (45)$$

$$\bar{\varphi}(k) = [r(k + n_{b-}) \quad u(k-1) \quad b]^T \quad (46)$$

$$A_2: \left\| (\bar{C}^* \bar{B}^*)^{-1} \{ \Delta\beta + \Delta B'(q^{-1}) + [(\bar{C}^* + \Delta C)(\bar{B}^* + \Delta B) + B_1(q^{-1}) + \Delta B_1(q^{-1})] \delta_1 \} \right\|_\infty \leq \beta < 1$$

$$\times \left\{ \frac{\alpha_1 \left\| \hat{\sigma} - \hat{\sigma}' \hat{W}_2^T \bar{\varphi} - 2\hat{\sigma}' \hat{W}_3^T q^{-1}(\hat{\sigma}) \right\|^2}{4} + \frac{\alpha_2 \left\| \hat{W}_1^T \hat{\sigma}' \right\|^2 \|\bar{\varphi}\|^2}{4} + \alpha_3 \left\| \hat{W}_1^T \hat{\sigma}' \right\|^2 \times \left\| q^{-1}(\hat{\sigma}) \right\|^2 + \frac{\alpha_4 \|\Psi\|^2}{4} \right\}. \quad (50)$$

The following theorem is the main theorem of the current paper and examines the properties of system (17) and (18) controlled by DNASMC (51)–(57).

*Theorem 1:* Consider the system (17) and (18) and the following controller:

$$u_n(k-d+1) = u_{eq}(k-d+1) + u_{sw}(k-d+1) \quad (51)$$

where we have (52) and (53), shown at the bottom of the page, where  $0 < \mu_5 > ((1-\beta)^2 / (1+\beta)^2) < 1$ . The amplitude of switching gains  $\phi(k) > 0$  is obtained from the following inequality:

$$\phi_2(k) > \phi(k) > \phi_1(k) \geq 0 \quad (54)$$

where

$$\phi_{1,2}(k) = \rho_1(k) \pm \sqrt{\rho_1^2(k) - \rho_2(k)} \quad (55)$$

$$\rho_1(k) = \frac{(1-\beta)^2 |s(k)|}{[(1+\beta)G_{sw}(k)]} - (1-\beta) \quad (56)$$

$$\rho_2(k) = (1-\beta)^2 \times \frac{\{G_{sw}^2(k) + 2G_{sw}(k)|s(k)| + \mu_5 s^2(k)\}}{G_{sw}^2(k)}. \quad (57)$$

If the overall system satisfies (A1) and (A2) and  $\left\| \tilde{W}_i(0) \right\|_F \leq W_{im}$ , then  $\left\{ \hat{W}_1(k), \hat{W}_2(k), \hat{W}_3(k), \hat{W}_4(k), s(k), u_n(k-d+1) \right\}$  are uniformly ultimately bounded (UUB), and the following performance (58) is achieved

$$D = \left\{ M(k) \in \mathfrak{R}^5 \mid 0 \leq \left\| \tilde{W}_i(k) \right\|_F \leq W_i^u, 1 \leq i \leq 4 \text{ and } 0 \leq |s(k)| \leq s^u \right\} \quad (58)$$

where we have (59)–(61), shown at the bottom of the page.

*Proof:* See the Appendix.

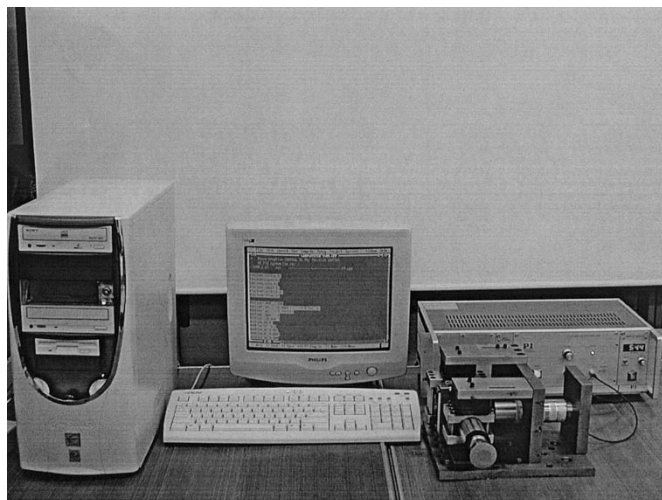
$$u_{eq}(k-d+1) = -(\bar{C}^* \bar{B}^*)^{-1} \left\{ \bar{C}^* \bar{A}^* \bar{G}^* Z(k) + (1-\rho) s(k) + \sum_{i=1}^{n_s} d_i e(k-i+1) \right\} - (\bar{C}^* \bar{B}^*)^{-1} \times \left\{ \hat{W}_1^T(k) \hat{\sigma}(k) + \left[ \Lambda_1^T(k) - \beta_1 \hat{W}_1^T(k) \right] \times \frac{\left[ \hat{\sigma}(k) - \hat{\sigma}'(k) \hat{W}_2^T(k) \bar{\varphi}(k) - 2\hat{\sigma}'(k) \hat{W}_3^T(k) q^{-1}(\hat{\sigma}) \right]}{2} + \hat{W}_1^T(k) \hat{\sigma}'(k) \left[ \frac{\Lambda_2^T(k)}{2} - \beta_2 \hat{W}_2^T(k) \right] \bar{\varphi}(k) + \hat{W}_1^T(k) \hat{\sigma}'(k) \left[ \Lambda_3^T(k) - 2\beta_3 \hat{W}_3^T(k) \right] q^{-1}(\hat{\sigma}) + \frac{\alpha_4 s(k) \Psi^T(k) \Psi(k)}{4} - \frac{(1-\beta_4) s(k) \hat{W}_4^T(k) \Psi(k)}{|s(k)|} \right\} \quad (52)$$

$$u_{sw}(k-d+1) = \begin{cases} \frac{-(\bar{C}^* \bar{B}^*)^{-1} \phi(k) G_{sw}(k) s(k)}{[(1-\beta)(1+\beta)|s(k)]}, & \text{if } \frac{|s(k)| > 2(1-\beta)(1+\beta)G_{sw}(k)}{[(1-\beta)^2 - (1+\beta)^2 \mu_5]} \\ 0, & \text{otherwise.} \end{cases} \quad (53)$$

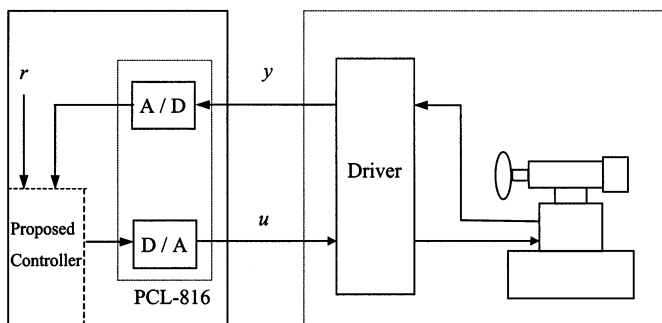
$$M(k) = \left[ \left\| \tilde{W}_1(k) \right\|_F \quad \left\| \tilde{W}_2(k) \right\|_F \quad \left\| \tilde{W}_3(k) \right\|_F \quad \left\| \tilde{W}_4(k) \right\|_F \quad |s(k)| \right] \quad (59)$$

$$W_i^u = \frac{[(1-\beta_i) + \sqrt{1-\mu_i}] \beta_i W_{im}}{[\beta_i(2-\beta_i) - \mu_i]}, \quad 1 \leq i \leq 4 \quad (60)$$

$$s^u > \frac{2(1-\beta)(1+\beta)G_{sw}(k)}{[(1-\beta)^2 - (1+\beta)^2 \mu_5]}. \quad (61)$$



(a)



Personal Computer

Piezomechanism

(b)

Fig. 4. Experimental setup of the overall system. (a) Photograph. (b) Control block diagram.

#### IV. EXPERIMENTS

In this section, we discuss the experimental setup, modeling, and experimental results.

##### A. Experimental Setup

The piezoelectric actuator system consists of two parts: 1) piezomechanism: piezotranslator, position sensor, driver, and carriage mechanism and 2) personal computer: AD/DA card and control program. The block diagram of the experimental setup is shown in Fig. 4. The carriage mechanism is made of steel for enhancing the strength of the mechanism. Four linear guides provided by THK Co. (Model no. VRU3088) are used to support the moving part of the mechanism. Furthermore, a high-speed spindle with weight 3.5 kg (Model no. PRECISE 3040) is fixed on the carriage mechanism. The piezotranslator is a Model no. P-246.70 from Physical Instrument (PI) Company. Its specifications are briefly described as follows: maximum expansion 120  $\mu\text{m}$ , electric capacitance 3000 nF, stiffness 190 N/ $\mu\text{m}$ , resonant frequency 3.5 kHz, and temperature expansion 2  $\mu\text{m}/\text{K}^\circ$ . The position signal is achieved from the position sensor (Model no. P-177.10 of PI Co.). The signal is sent to a 16 bit A/D card (PCL-816) in an 80 586 personal computer. Together with a reference input in the computer program written by Turbo C, the

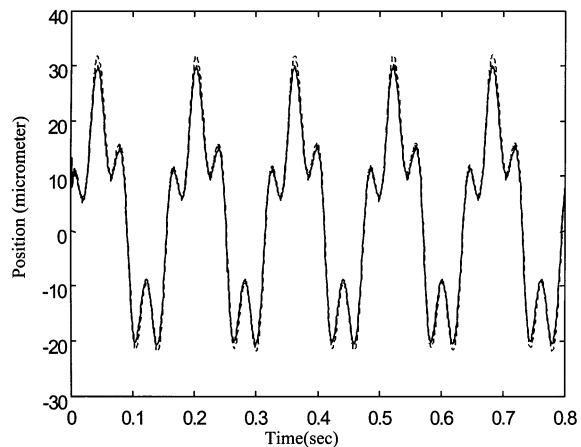


Fig. 5. Output responses of the system (...) and mathematical model (—) using the input  $3 + 24 \sin(10\pi k) + 12 \cos(40\pi k) \mu\text{m}$  for the model.

control signal  $u(k)$  is calculated. The control input through the D/A card is then sent to the driver (Model no. P-271.10 from PI Co.). The output voltage of driver, between  $-200$  and  $1000$  V, is employed to drive the piezotranslator. The different position signal is accomplished by using a different input signal. The process is repeated until the total process time is over. The time required for every process is called the “control cycle time ( $T_c = 0.0008$  s).”

##### B. Modeling

Based on the offline learning of the piezoelectric actuator, the nominal coefficients of (2) and (3) are described as follows:

$$\begin{aligned} \bar{a}_1^* &= 0.303147, & \bar{a}_2^* &= 0.283635, & \bar{a}_3^* &= 0.175854; \\ \bar{b}_1^* &= 1.225019, & \bar{b}_2^* &= -0.498813, & \bar{b}_3^* &= 0.933854 \\ \bar{c}_{p1}^* &= -0.015012, & \bar{c}_{p2}^* &= 0.775711, & \bar{c}_{p3}^* &= 1.491532 \\ \bar{c}_{n1}^* &= -0.110386, & \bar{c}_{n2}^* &= -0.25888, & \bar{c}_{n3}^* &= -0.48270. \end{aligned}$$

The proposed piezoelectric actuator is generally used for the frequency range 0–30 Hz and the amplitude range  $\pm 50 \mu\text{m}$ . Based on the application, the signal with the frequencies 0, 5, and 20 Hz, and the amplitude between  $-27$  and  $38 \mu\text{m}$  is assumed as the input for the model verification. The corresponding result of the model verification is shown in Fig. 5 that the maximum modeling error is about 10% of the maximum amplitude of the input signal. It is acceptable because the NIC is used for many different amplitudes or frequencies of the reference input. The remaining uncertainty is then tackled by the DNASMC.

##### C. Experimental Results

The reference input is assigned as  $r(k) = 3 + 24 \sin(10\pi k) + 12 \cos(40\pi k) \mu\text{m}$  consisting of frequencies 0, 5, and 20 Hz. In addition, the open-loop response of the piezoelectric actuator system for this reference input is presented in Fig. 6. Its maximum tracking error is about 31.5% of the maximum amplitude of the reference input. It indicates that the response of the open-loop system is poor.

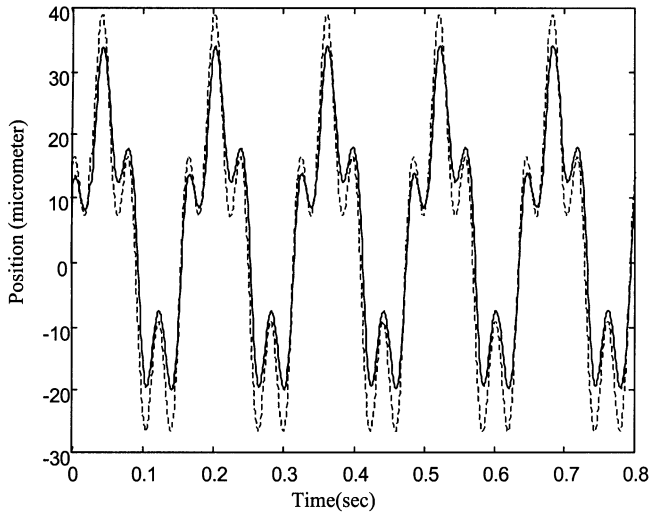


Fig. 6. Open-loop response of the piezoelectric actuator (—) for the reference input  $3 + 24 \sin(10\pi k) + 12 \cos(40\pi k) \mu\text{m}$  (...).

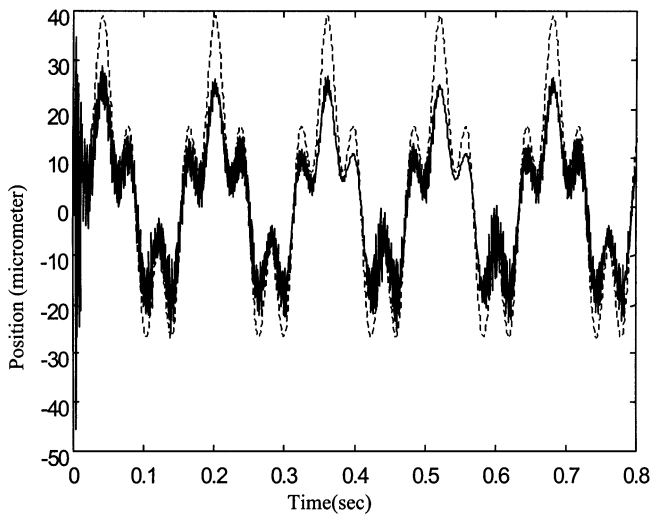


Fig. 7. Output response of the PID (—) control for the reference input  $3 + 24 \sin(10\pi k) + 12 \cos(40\pi k) \mu\text{m}$  (...).

In addition, the PID controller is applied to control the piezoelectric actuator system for this reference input. The form of the discrete-time PID controller is expressed as follows (cf. [6]):

$$u(k) = K_p e(k) + K_p \frac{T_c}{T_I} \sum e(k) + K_p \frac{T_D}{T_c} [e(k) - e(k-1)]. \quad (62)$$

The output response of only PID control with  $K_p = 2.0$ ,  $T_I = 15$ , and  $T_D = 0.0001$  is shown in Fig. 7 that is oscillatory. Because the piezoceramic materials are ferroelectric, they have inherent nonlinearity and hysteresis. If the parameter  $K_p$  is selected too high, the oscillation becomes grave. The other selections of control parameters for (62) have a similar response of Fig. 7.

Sequentially, the output response by using the forward control (NIC) is presented in Fig. 8; its maximum tracking error is about 19.4% of the maximum amplitude of the reference input. The main reason is that only use of NIC cannot achieve an excellent tracking result as the system is subject to the uncertain-

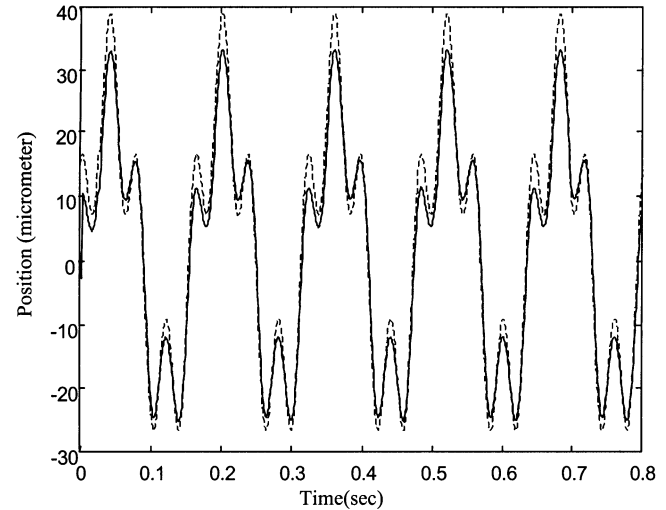


Fig. 8. Output response of the NIC (—) for the reference input  $3 + 24 \sin(10\pi k) + 12 \cos(40\pi k) \mu\text{m}$  (...).

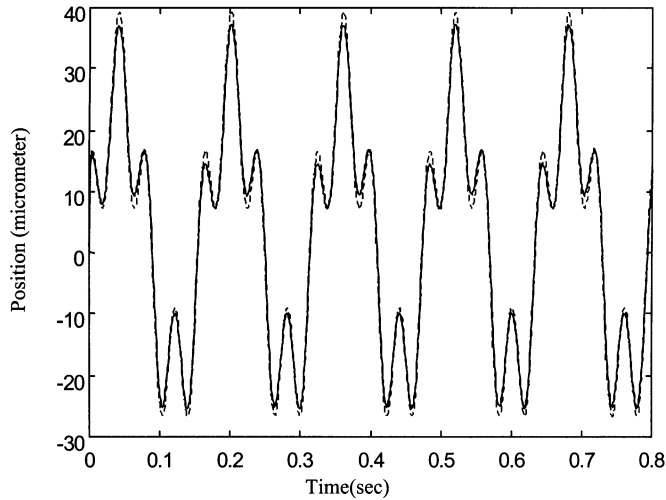


Fig. 9. Output response of the NIC and PID control (—) for the reference input  $3 + 24 \sin(10\pi k) + 12 \cos(40\pi k) \mu\text{m}$  (...).

ties caused by different polarities or frequencies of the reference input. In this situation, the output response by using the forward control (NIC) and PID control (62) with  $K_p = 1.1$ ,  $T_I = 15$ ,  $T_D = 0.0001$  is shown in Fig. 9. Because the hysteretic behavior of the piezoelectric actuator system is canceled by the forward control, the tracking control performance is better than that using only the PID control (62) (cf. Figs. 7 and 9). However, its maximum tracking error is about 9.8% of the maximum amplitude of the reference input that is still large.

Under the circumstances, the proposed DNASMC is applied to reinforce the system performance. The sliding surface is first selected as follows:  $s(k) = s(k-1) + e(k) - 0.3e(k-1) + 0.02e(k-2)$ . The control parameters are chosen as follows:  $\mu_5 = 0.2$ ,  $\alpha = 11$ ,  $b = 1$ ,  $\alpha_1 = 0.8936$ ,  $\alpha_2 = 0.002$ ,  $\alpha_3 = 0.001$ ,  $\alpha_4 = 0.0165$  (learning rate) and  $\beta_1 = 0.935$ ,  $\beta_2 = 0.025$ ,  $\beta_3 = 0.06$ ,  $\beta_4 = 0.32$  (e-modification rate). The response of the proposed control is then shown in Fig. 10. As compared to the performance of the NIC and PID control, the tracking performance of Fig. 10(a) is indeed much better than that of Figs. 8 and

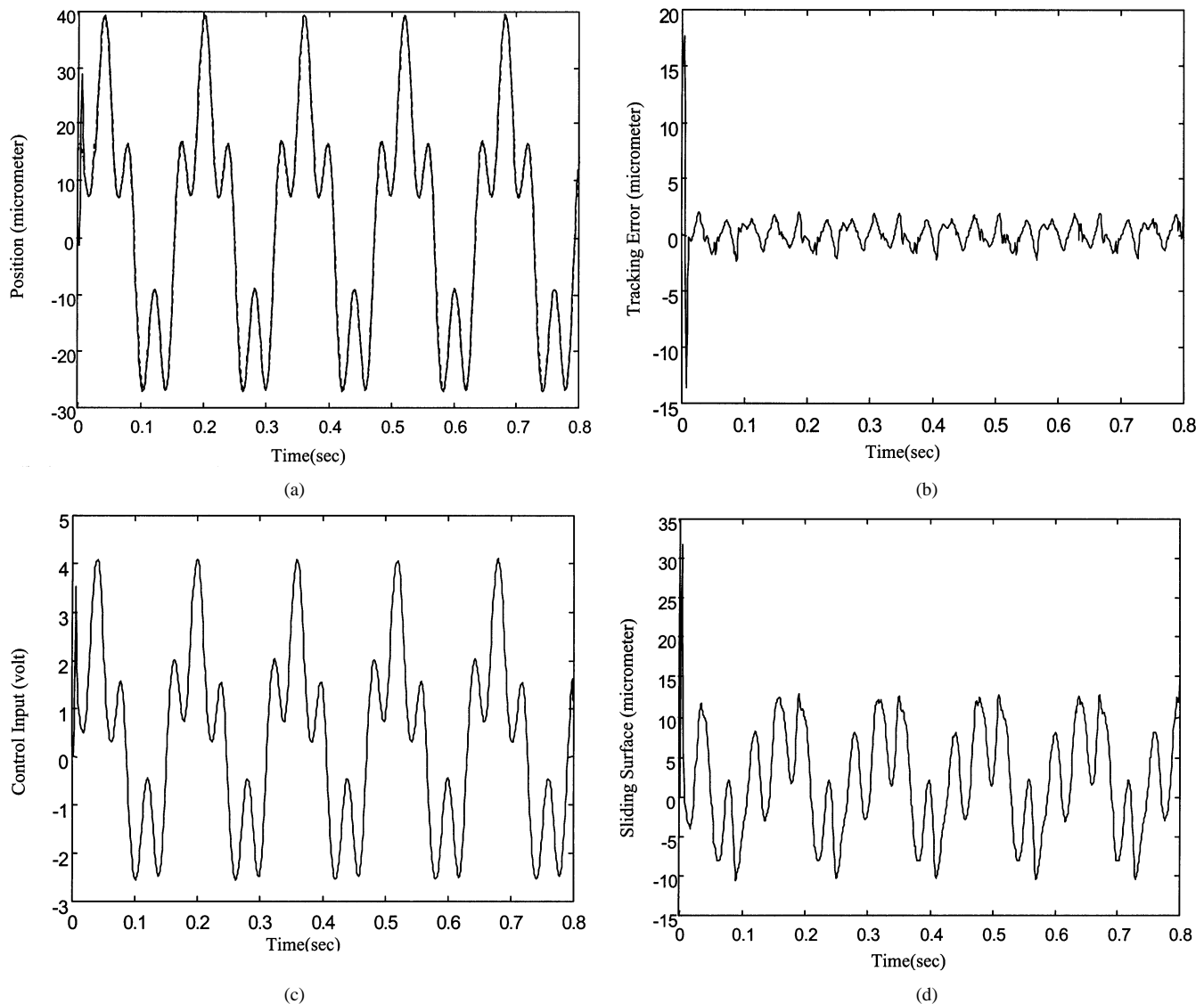


Fig. 10. (a) The output response of the proposed control (—) for the reference input  $3 + 24 \sin(10\pi k) + 12 \cos(40\pi k) \mu\text{m}$  (...). (b) The tracking error response of the proposed control for the reference input  $3 + 24 \sin(10\pi k) + 12 \cos(40\pi k) \mu\text{m}$ . (c) The control input response of the proposed control for the reference input  $3 + 24 \sin(10\pi k) + 12 \cos(40\pi k) \mu\text{m}$ . (d) The sliding surface response of the proposed control for the reference input  $3 + 24 \sin(10\pi k) + 12 \cos(40\pi k) \mu\text{m}$ .

9. For clearness, its corresponding tracking error is shown in Fig. 10(b); its maximum steady-state tracking error is about 4.9% of the maximum amplitude of the reference input. Fig. 10(c) shows the corresponding control input that is smooth enough. The corresponding response of the sliding surface is shown in Fig. 10(d). The performances for the other control parameters are similar with the results of Fig. 10. Due to space considerations, those are omitted. In short, once a suitable set of control parameters are obtained from the simulation, the selection of them is not critical. For simplicity, the corresponding simulations are not presented.

## V. CONCLUSION

The proposed controller includes an NIC based on a learned nonlinear model and a DNASMC based on an on-line approximation of huge dynamic uncertainties by using an RNN. The proposed RNN possesses the residue compensation of the uncertainty caused by the learning. The features of the nonlinear

model and the network have their necessities and advantages. Without the risk of discontinuous response, the NIC cancels the hysteretic phenomenon and tracks the reference input in an acceptable manner. Furthermore, a DNASMC does not need the state estimator. This is the first time to use the aforementioned concepts for the control of the piezoelectric actuator with dominant hysteresis. The comparisons among the open-loop control, the PID control, the NIC, the NIC + PID control, and the proposed control, are also given to verify the usefulness of the proposed control. From the experimental results, the proposed control effectively deals with a class of systems having dominant hysteresis. The trajectory to be tracked is not limited to a sinusoidal signal. The authors believe that the proposed control can be applied to many other control problems.

## APPENDIX

Without ambiguity, the arguments of variables in the following appendixes are omitted.

Define the following Lyapunov function:

$$V(\tilde{W}_1, \tilde{W}_2, \tilde{W}_3, \tilde{W}_4, s) = \frac{\sum_{i=1}^4 \text{tr}[\tilde{W}_i^T \tilde{W}_i]}{\alpha_i} + \frac{s^2}{2} = M^T P M \quad (\text{A1})$$

where  $P = \text{diag}[1/\alpha_1 \ 1/\alpha_2 \ 1/\alpha_3 \ 1/\alpha_4 \ 1/2]$ .

1) The case of  $P_i = \beta_i \tilde{W}_i$  is first investigated.

From (40) and (A1), the change rate of  $V(\tilde{W}_1, \tilde{W}_2, \tilde{W}_3, \tilde{W}_4, s)$  is described as shown in (A2), shown at the bottom of the page, where  $\Delta V_5 = \Delta s^2/2 + s\Delta s$ . Using (39), (17), (25), (51) and (52) gives the following  $\Delta s$  in (A3), shown at the bottom of the page, where the third and fourth equalities have used the facts  $X(k) = \bar{C}^* Z(k) + \Delta G(e, u_n, r)$  and  $X(k) = C^p [e(k) - e_{ze}(k) - d_e(k)]$ , respectively,  $R_{sw}(k)$  is shown in (54), and

$$\begin{aligned} \Pi = & 1 + (\bar{C}^* \bar{B}^*)^{-1} \\ & \times \{ \Delta\beta + \Delta B' + [(\bar{C}^* + \Delta C)(\bar{B}^* + \Delta B) \\ & + B' + \Delta B'] \delta_1 \}. \end{aligned} \quad (\text{A4})$$

Assume that  $\Delta V_5 \leq -\mu_5 V_5$  (or  $\Delta \bar{V}_5 < 0$ ) where  $0 < \mu_5 > (1 - \beta)^2 / (1 + \beta)^2 < 1$ . Then, the fol-

lowing equation is achieved by using (53) for  $|s| > 2(1 - \beta)(1 + \beta)G_{sw} / [(1 - \beta)^2 - (1 + \beta)^2 \mu_5]$ , the inequalities  $\Pi^2 / (1 + \beta)^2 < 1$ ,  $\Pi / (1 - \beta) > 1$ , and assumption (A2).

$$\begin{aligned} \Delta \bar{V}_5 = & (\bar{C}^* \bar{B}^*)^2 \frac{\Pi^2 u_{sw}^2}{2} + (\bar{C}^* \bar{B}^*) R_{sw} \Pi u_{sw} \\ & + \frac{R^2}{2} + s(\bar{C}^* \bar{B}^*) \Pi u_{sw} + s R_{sw} + \frac{\mu_5 s^2}{2} \\ \leq & \frac{\phi^2 G_{sw}^2}{2(1 - \beta)^2} + \frac{\phi G_{sw}^2}{(1 - \beta)} + \frac{G_{sw}^2}{2} \\ & - \frac{\phi |s| G_{sw}}{(1 + \beta)} + |s| G_{sw} + \frac{\mu_5 |s|^2}{2} \\ = & G_{sw}^2 \frac{\{\phi^2 - 2\rho_1 \phi + \rho_2\}}{[2(1 - \beta)^2]} \end{aligned} \quad (\text{A5})$$

where the expressions of  $\rho_1$  and  $\rho_2$  are shown in (55) and (56). Because  $|s| > 2(1 - \beta)(1 + \beta)G_{sw} / [(1 - \beta)^2 - (1 + \beta)^2 \mu_5]$ ,  $\rho_1 > 0$  and  $\rho_1^2 - \rho_2 > 0$ . The result (54) is achieved from the inequality  $\phi^2 - 2\rho_1 \phi + \rho_2 < 0$ . In short, the switching gain chosen from (54) makes  $\Delta V_5 \leq -\mu_5 V_5$ . Furthermore, from

$$\Delta V = \sum_{i=1}^5 \Delta V_i = \sum_{i=1}^4 \text{tr} \frac{\left[ (\tilde{W}_i - \Lambda_i + \beta_i \hat{W}_i)^T (\tilde{W}_i - \Lambda_i + \beta_i \hat{W}_i) - \tilde{W}_i^T \tilde{W}_i \right]}{\alpha_i} + \frac{\Delta s^2}{2} + s\Delta s \quad (\text{A2})$$

$$\begin{aligned} \Delta s = & \sum_{i=0}^{n_s} d_i e(k - i + 1) - (1 - \rho)s(k) = (\bar{C}^* + \Delta C) \\ & \times [(\bar{A}^* + \Delta A) X(k) + (\bar{B}^* + \Delta B)(u_n(k - d + 1) + e_h(k - d + 1))] \\ & - e_{ze}(k + 1) - d_e(k + 1) + \sum_{i=1}^{n_s} d_i e(k - i + 1) - (1 - \rho)s(k) \\ = & \bar{C}^* \bar{A}^* \bar{G}^* Z(k) + \bar{C}^* \bar{B}^* u_n(k - d + 1) + \sum_{i=1}^{n_s} d_i e(k - i + 1) \\ & + [\Delta C \bar{A}^* + \bar{C}^* \Delta A + \Delta C \Delta A] X(k) \\ & + (\bar{C}^* + \Delta C)(\bar{B}^* + \Delta B)(e_{ze}(k) + d_e(k)) + \Delta \beta u_{eq}(k - d + 1) \\ & + \Delta \beta u_{sw}(k - d + 1) - \bar{a}_1^* \Delta g_1(k) + \Delta g_2(k) \\ = & (\bar{C}^* \bar{B}^*) \Pi u_{sw}(k - d + 1) + \Gamma_u(k) - \hat{W}_1^T(k) \hat{\sigma}(k) \\ & + \frac{\Lambda_1^T(k) [\hat{\sigma} - \hat{\sigma}'(k) \hat{W}_2^T(k) \bar{\varphi}(k) - 2\hat{\sigma}(k) \hat{W}_3^T(k) q^{-1}(\hat{\sigma})]}{2} + \frac{\hat{W}_1^T(k) \hat{\sigma}'(k) \Lambda_2^T(k) \bar{\varphi}(k)}{2} \\ & + \frac{\hat{W}_1^T(k) \hat{\sigma}'(k) \Lambda_3^T(k) q^{-1}(\hat{\sigma})}{2} + \frac{\alpha_4 s(k) \Psi^T(k) \Psi(k)}{4} - \frac{s(k) \hat{W}_4^T(k) \Psi(k)}{|s(k)|} \\ = & (\bar{C}^* \bar{B}^*) \Pi u_{sw}(k - d + 1) + R_{sw}(k) \end{aligned} \quad (\text{A3})$$

(A2), we have (A6) at the bottom of the page. Based on the mathematical preliminary of  $\text{tr}\{\cdot\}$  operator and (41)–(44), the following equalities are achieved:

$$\begin{aligned}
s\tilde{W}_1^T \left[ \hat{\sigma} - \hat{\sigma}' \hat{W}_2^T \bar{\varphi} - 2\hat{\sigma}' \hat{W}_3^T q^{-1}(\hat{\sigma}) \right] &= \frac{2\text{tr} \left[ \tilde{W}_1^T \Lambda_1 \right]}{\alpha_1} \\
s\hat{W}_1^T \hat{\sigma}' \tilde{W}_2^T \bar{\varphi} &= \frac{2\text{tr} \left[ \tilde{W}_2^T \Lambda_2 \right]}{\alpha_2} \\
2s\hat{W}_1^T \hat{\sigma}' \tilde{W}_3^T q^{-1}(\hat{\sigma}) &= \frac{2\text{tr} \left[ \tilde{W}_3^T \Lambda_3 \right]}{\alpha_3} \\
s \left( \frac{\Lambda_1^T}{2} - \beta_1 \right) \left[ \hat{\sigma} - \hat{\sigma}' \hat{W}_2^T \bar{\varphi} - 2\hat{\sigma}' \hat{W}_3^T q^{-1}(\hat{\sigma}) \right] \\
&= \frac{\left\{ \text{tr} \left[ \Lambda_1^T \Lambda_1 \right] \right\}}{\alpha_1} \\
s\hat{W}_1^T \hat{\sigma}' \left( \frac{\Lambda_2^T}{2} - \beta_2 \right) \bar{\varphi} &= \frac{\left\{ \text{tr} \left[ \Lambda_2^T \Lambda_2 \right] \right\}}{\alpha_2} \\
s\hat{W}_1^T \left( \Lambda_3^T - 2\beta_3 \right) \hat{\sigma}' q^{-1}(\hat{\sigma}) &= \left\{ \text{tr} \left[ \Lambda_3^T \Lambda_3 \right] \right\} \alpha_3 \\
s(1 - \beta_4) \frac{\alpha_4 s \Psi^T \Psi}{4} &= \frac{\left\{ \text{tr} \left[ \Lambda_4^T \Lambda_4 \right] \right\}}{\alpha_4}. \tag{A7}
\end{aligned}$$

Moreover, the following inequalities are attained from (44) and (38).

$$\begin{aligned}
s \left[ \tilde{\varepsilon}_f - \frac{s\hat{W}_4^T \Psi}{|s|} \right] - \frac{2\text{tr} \left[ \tilde{W}_4^T \Lambda_4 \right]}{\alpha_4} \\
\leq |s| \|\tilde{\varepsilon}_f\| - |s| \hat{W}_4^T \Psi - |s| \tilde{W}_4^T \Psi \leq 0. \tag{A8}
\end{aligned}$$

Suppose that  $\Delta V_i \leq -\mu_i V_i$  for  $1 \leq i \leq 4$ . If  $\|\tilde{W}_i\|_F \geq [(1 - \beta_i) + \sqrt{1 - \mu_i}] \beta_i W_{im} / [\beta_i(2 - \beta_i) - \mu_i]$ , then the following result is achieved from (A6)–(A8).

See (A9) at the bottom of the page, where  $\beta_i(2 - \beta_i) - \mu_i > 0$ ,  $1 > \beta_i > \mu_i > 0$ . Hence,

$$\Delta V \leq - \sum_{i=1}^5 \mu_i V_i \leq - \min_{1 \leq i \leq 5} (\mu_i) V = -\mu V \tag{A10}$$

where  $0 < \mu < 1$ . Hence, outside of the domain  $D$  in (63) making  $\Delta V \leq -\mu V$  is accomplished.

2) Then, the case of  $P_i = \beta_i \hat{W}_i + \text{tr} \left[ \Lambda_i^T \hat{W}_i \right] / \left[ \gamma + \|\hat{W}_i\|_F^2 \right]$  is examined as follows.

The above results in (A6) have the extra second term in the right-hand side of (48). See equation (A11) at the bottom of the page, where

$$\begin{aligned}
F_i &= \frac{\text{tr} \left[ \tilde{W}_i^T \hat{W}_i \right] \text{tr} \left[ \left( \Lambda_i - \beta_i \hat{W}_i \right)^T \hat{W}_i \right]}{\left( \gamma + \|\hat{W}_i\|_F^2 \right)} \\
&\quad - \frac{2\text{tr} \left[ \left( \Lambda_i - \beta_i \hat{W}_i \right)^T \hat{W}_i \right]^2}{\left( \gamma + \|\hat{W}_i\|_F^2 \right)} \\
&\quad + \frac{\text{tr} \left[ \left( \Lambda_i - \beta_i \hat{W}_i \right)^T \hat{W}_i \right]^2 \text{tr} \left[ \hat{W}_i^T \hat{W}_i \right]}{\left( \gamma + \|\hat{W}_i\|_F^2 \right)^2}. \tag{A12}
\end{aligned}$$

$$\Delta V_i = \frac{\left\{ -2\text{tr} \left[ \tilde{W}_i^T \Lambda_i \right] + 2\beta_i \text{tr} \left[ \tilde{W}_i^T \hat{W}_i \right] + \text{tr} \left[ \Lambda_i^T \Lambda_i \right] - 2\beta_i \text{tr} \left[ \hat{W}_i^T \Lambda_i \right] + \beta_i^2 \text{tr} \left[ \hat{W}_i^T \hat{W}_i \right] \right\}}{\alpha_i}, \text{ for } 1 \leq i \leq 4. \tag{A6}$$

$$\begin{aligned}
\Delta \bar{V}_i &= \Delta V_i + \mu_i V_i = \frac{- \left\{ [\beta_i(2 - \beta_i) - \mu_i] \|\tilde{W}_i\|_F^2 - 2\beta_i(1 - \beta_i) W_{im} \|\tilde{W}_i\|_F - \beta_i^2 W_{im}^2 \right\}}{\alpha_i} \\
&= - [\beta_i(2 - \beta_i) - \mu_i] \left\{ \left[ \|\tilde{W}_i\|_F - \frac{\beta_i(1 - \beta_i) W_{im}}{\beta_i(2 - \beta_i) - \mu_i} \right]^2 - \frac{(1 - \beta_i) \beta_i^2 W_{im}^2}{[\beta_i(2 - \beta_i) - \mu_i]^2} \right\} \leq 0 \tag{A9}
\end{aligned}$$

$$\Delta V_i \leq - \frac{\left\{ \beta_i(2 - \beta_i) \|\tilde{W}_i\|_F^2 - 2\beta_i(1 - \beta_i) W_{im} \|\tilde{W}_i\|_F - \beta_i^2 W_{im}^2 \right\}}{\alpha_i} + F_i \leq \mu_i V_i \tag{A11}$$

Based on the definition of  $\tilde{W}_i = \bar{W}_i - \hat{W}_i$  and  $\text{tr}[\cdot]$  operator

$$\begin{aligned}
 \text{tr}[\tilde{W}_i^T \hat{W}_i] &= \text{tr}\left[\left(\bar{W}_i - \hat{W}_i\right)^T \hat{W}_i\right] \\
 &= \text{tr}\left[\bar{W}_i^T \hat{W}_i - \frac{\hat{W}_i^T \hat{W}_i}{2} - \frac{\hat{W}_i^T \hat{W}_i}{2}\right] \\
 &= \text{tr}\left[\bar{W}_i^T \left(\bar{W}_i - \tilde{W}_i\right) - \frac{\left(\bar{W}_i - \tilde{W}_i\right)^T \left(\bar{W}_i - \tilde{W}_i\right)}{2} - \frac{\hat{W}_i^T \hat{W}_i}{2}\right] \\
 &= \text{tr}\left[\frac{\bar{W}_i^T \bar{W}_i}{2} - \frac{\tilde{W}_i^T \tilde{W}_i}{2} - \frac{\hat{W}_i^T \hat{W}_i}{2}\right] \\
 &= -\frac{\left[\left\|\tilde{W}_i\right\|_F^2 + \left\|\hat{W}_i\right\|_F^2 - \left\|\bar{W}_i\right\|_F^2\right]}{2}. \quad (\text{A13})
 \end{aligned}$$

Then from (A12) and (A13)  $F_i < 0$ , if  $\left\|\hat{W}_i\right\|_F \geq W_{im}$  and  $\text{tr}\left[\left(\Lambda_i - \beta_i \hat{W}_i\right)^T \hat{W}_i\right] > 0$ . That is, the projection algorithm (40) of second case makes  $\Delta V_i + \mu_i V_i \leq 0$  of the first case more negative. Because  $0 \leq \left\|\hat{W}_i(0)\right\| \leq W_{im}$ , and the constant value  $0 \leq \left\|\bar{W}_i\right\| \leq W_{im}$  exists, then  $\left\|\hat{W}_i\right\| \leq W_{im}$  as  $k \rightarrow \infty$ .

Q. E. D.

#### REFERENCES

- [1] A. B. Palazzolo, S. Jagannathan, A. F. Kascak, G. T. Montague, and L. J. Kiraly, "Hybrid active vibration control of rotor bearing systems using piezoelectric actuators," *Trans. ASME J. Vibr., Acoust.*, vol. 115, pp. 111–119, 1993.
- [2] S. B. Jung and S. W. Kim, "Improvement of scanning accuracy of PZT piezoelectric actuator by feed-forward model-reference control," *Prec. Eng.*, vol. 16, no. 1, pp. 49–55, 1994.
- [3] G. Tao and P. V. Kokotovic, "Adaptive control of plants with unknown hysteresis," *IEEE Trans. Automat. Contr.*, vol. 40, pp. 200–212, Feb. 1995.
- [4] H. R. Pota and T. E. Alberts, "Multivariable transfer functions for a slewing piezoelectric laminate beam," *Trans. ASME J. Dyna. Syst., Meas., Contr.*, vol. 117, pp. 352–359, 1995.
- [5] J. D. Kim and S. R. Nam, "Development of a micro-positioning grinding table using piezoelectric voltage feedback," *IME Proc. I, J. Syst., Contr. Eng.*, vol. 209, pp. 469–474, 1995.
- [6] P. Ge and M. Jouaneh, "Tracking control of a piezoceramic actuator," *IEEE Trans. Contr. Syst. Technol.*, vol. 4, pp. 209–216, May 1996.
- [7] J. M. Cruz-Hernandez and V. Hayward, "Reduction of major and minor hysteresis loops in a piezoelectric actuator," in *37th IEEE Conf. Decision Control*, Tampa, FL, USA, 1998, pp. 4320–4325.
- [8] J. F. Cuttino, A. C. Miller, and D. E. Schinstock, "Performance of a fast tool servo for single-point diamond turning machines," *IEEE/ASME Trans. Mechatron.*, vol. 4, pp. 169–179, June 1999.
- [9] K. Y. Tsai and J. Y. Yen, "Servo system design of a high-resolution piezo-driven fine stage for step-and-repeat microlithography systems," in *Proc. IEEE IECON'99*, vol. 1, 1999, pp. 11–16.

- [10] C. L. Hwang, C. Jan, and Y. H. Chen, "Piezomechanics using intelligent variable structure control," *IEEE Trans. Ind. Electron.*, vol. 48, pp. 47–59, Jan. 2001.
- [11] J. B. D. Cabera and K. S. Narendra, "Issues in the application of neural networks for tracking based on inverse control," *IEEE Trans. Automat. Contr.*, vol. 44, pp. 2007–2027, Nov. 1999.
- [12] C. L. Hwang and C. H. Lin, "A discrete-time multivariable neuro-adaptive control for nonlinear unknown dynamic systems," *IEEE Trans. Syst., Man, Cybern. B*, vol. 30, no. 6, pp. 865–877, 2000.
- [13] C. C. Ku and K. Y. Lee, "Diagonal recurrent neural networks for dynamic systems control," *IEEE Trans. Neural Networks*, vol. 6, pp. 144–156, Jan. 1995.
- [14] M. K. Sundareshan and T. A. Condarcuru, "Recurrent neural-network training by a learning automation approach for trajectory learning and control system design," *IEEE Trans. Neural Networks*, vol. 9, pp. 354–368, May. 1998.
- [15] D. Jiang and J. Wang, "On-line learning of dynamical systems in the presence of model mismatch and disturbances," *IEEE Trans. Neural Networks*, vol. 11, pp. 1272–1283, Nov. 2000.
- [16] H. K. Khalil, *Nonlinear Systems*, 2nd ed. Upper Saddle River, NJ: Prentice-Hall, 1996.
- [17] K. J. Astrom and B. Wittenmark, *Computer-Controlled Systems—Theory and Design*, 3rd ed. Upper Saddle River, NJ: Prentice-Hall, 1997.



**Chih-Lyang Hwang** received the B.E. degree in aeronautical engineering from Tamkang University, Taipei, Taiwan, R.O.C., in 1981, the M.E. and Ph.D. degrees in mechanical engineering from Tatung Institute of Technology, Taipei, Taiwan, R.O.C., in 1986 and 1990, respectively.

Since 1990, he has been with the Department of Mechanical Engineering, Tatung Institute of Technology, where he is engaged in teaching and research in the area of servo control and control of manufacturing systems. Since 1996, he has been a

Professor of Mechanical Engineering of Tatung Institute of Technology. He is a Technical Committee Member of IEEE IECON'02. From 1998 to 1999, he was a Research Scholar with the George W. Woodruff School of Mechanical Engineering, Georgia Institute of Technology, Atlanta. He is the author or coauthor of about 60 journal and conference papers in the related field. His current research interests include fuzzy (neural-network) modeling and control, variable structure control, mechatronics, robotics, and visual servo systems.

Dr. Hwang received a number of awards, including the Excellent Research Paper Award from the National Science Council of Taiwan and Hsieh-Chih Industry Renaissance Association of Tatung Company.



**Chau Jan** was born in Taiwan, R.O.C., in 1972. He received the B.E. degree from the Department of Mechanical Engineering, National Cheng Kung University, Tainan, Taiwan, R.O.C., and the M.E. degree from Tatung University, Taipei, Taiwan, R.O.C., both in mechanical engineering, in 1996 and 1998, respectively. He is currently working toward the Ph.D. degree in mechanical engineering at Tatung University.

His current research interests include control system, robust control, neural networks, fuzzy logic theory, piezomechanics, and dynamic systems.